

Contents lists available at ScienceDirect

Acta Materialia

journal homepage: www.elsevier.com/locate/actamat



Full length article

Nanotwinning and amorphization of boron suboxide

Cody Kunka ^a, Qi An ^b, Nicholas Rudawski ^c, Ghatu Subhash ^{a, *}, James Zheng ^d, Virginia Halls ^d, Jogender Singh ^e

- ^a Mechanical and Aerospace Engineering, University of Florida, Gainesville, FL, 32611, USA
- ^b Chemical and Materials Engineering, University of Nevada, Reno, Reno, NV, 89557, USA
- ^c Herbert Wertheim College of Engineering Research Service Centers, Gainesville, FL, 32611, USA
- ^d PEO Soldier, Fort Belvoir, VA, 22060, USA
- ^e Penn State University, State College, PA, 16801, USA



ARTICLE INFO

Article history:
Received 11 October 2017
Received in revised form
10 January 2018
Accepted 12 January 2018
Available online 3 February 2018

Keywords:
Nanotwinning
Boron suboxide
Boron carbide
Amorphization
Density functional theory

ABSTRACT

Recently, researchers discovered that in contrast to isolated twins, periodic twins with nanoscale spacing can dramatically improve mechanical properties. Ceramics engineers now seek to incorporate this "nanotwinning" into icosahedral solids because of their high strength, high stability, and low mass density. In this manuscript, we assert that boron suboxide, while far less studied than boron carbide (i.e., the most popular icosahedral solid), possesses higher propensity for nanotwinning and higher theoretical promise. For boron suboxide, the influence of processing on twin spacing is explored through mechanical testing and transmission electron microscopy. Quantum-mechanical simulations are then performed to suggest a critical twin spacing that would maximize performance and to show how to track experimental nanotwinning with x-ray diffraction. Finally, transmission electron microscopy and Raman spectroscopy show that amorphization, the localized loss of crystallinity, drives mechanical failure in ways unique to boron suboxide.

© 2018 Acta Materialia Inc. Published by Elsevier Ltd. All rights reserved.

1. Introduction

Twins are crystallographic defects represented by a reflection of a parent lattice. They can occur during nucleation, growth, phase transformation, recrystallization, annealing, or deformation. Regardless of origin, twins generally induce stress concentrations that promote crack nucleation and lower mechanical performance [1]. However, recent investigations showed that increasing twin density (i.e., reducing twin spacing, λ) at the nanoscale can dramatically increase mechanical properties even beyond those of nanograined structures [2,3]. Nanotwinned copper (nt-Cu) produced by pulsed electrodeposition exhibited an order-ofmagnitude increase in yield strength over regular copper (i.e., 900 vs. 70 MPa) without lowering electrical conductivity [4,5]. A later study showed nt-Cu had up to an 85% increase in fatigue strength (i.e., 370 vs. 80 MPa) [6]. Nanotwinned cubic boron nitride (nt-c-BN, $\lambda \approx 3.8 \, nm$) produced from onion nanoparticles exhibited a 40% increase in microhardness (>100 GPa) and a 140% increase in

* Corresponding author. E-mail address: subhash@ufl.edu (G. Subhash). fracture toughness (>12 MPa m^{1/2}) [7,8]. Also produced from onion nanoparticles, nanotwinned diamond (nt-D, $\lambda \approx 5$ nm) reached a 200-GPa record hardness and showed improved thermal stability [9].

The latest proposals for nanotwinning are two ceramics: boron carbide (nt-B₄C) [10–12] and boron suboxide (nt-B₆O or β -B₆O) [13–15]. Experimentally, both B₄C and B₆O have exhibited superhardness (i.e., microhardness above 40 GPa), low mass density (2.52 g/cm³ for B₄C and 2.60 g/cm³ for B₆O), and moderate fracture toughness (3.4 MPa m^{1/2} for B₄C and 4.2 MPa m^{1/2} for B₆O) [16–20]. Crystallographically, these materials share boron-based icosahedra but have important differences [see Fig. 1(a) and (b)]. B₄C has threeatom chains that connect icosahedra, but the oxygen atoms that bond icosahedra in B₆O do not form chains. Icosahedral carbons can break the sixfold-symmetry in B₄C but not in B₆O. Also, B₄C is highly susceptible to structural heterogeneity due to polymorphism [17,21] while B₆O is not [16]. These differences in crystal structure affect the orientation of planar defects, such as twins. In B_6O , the $\{100\}_r$ family of planes is preferred for twinning [14,15,22] while many factors, such as stoichiometry and processing, strongly affect the preferred planes in B₄C [12,23,24]. As explained later, we believe these differences make B₆O more structurally

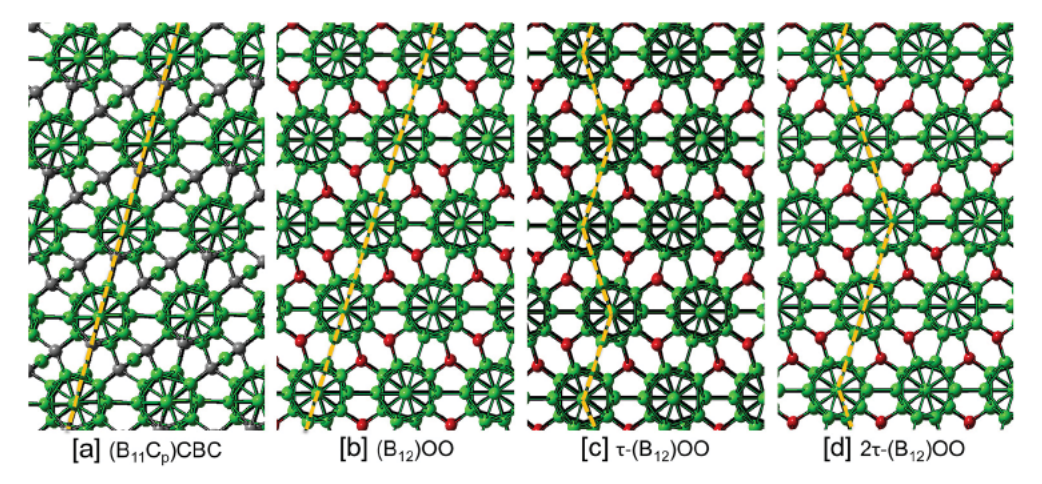


Fig. 1. The crystal structures of (a) $(B_{11}C_p)CBC$, (b) α -B₆O, (c) τ -B₆O, and (d) 2τ -B₆O share icosahedral fundamental units. Spheres are colored by element (i.e., green for boron, grey for carbon, and red for oxygen) and are sized according to covalent radius. Bends in the dashed yellow lines indicate twin planes. Note that the (a) C-B-C linear chains in B₄C are serially bonded while the (b-d) oxygen atoms in B₆O do not form chains. (For interpretation of the references to color in this figure legend, the reader is referred to the Web version of this article.)

homogeneous and therefore a better candidate for nanotwinning. Hence, this manuscript focuses on B_6O but compares to B_4C when warranted.

Just as nanograining has a critical grain size that maximizes mechanical strength (i.e., Hall-Petch relationship), nanotwinning has a critical twin spacing (λ_{cr}). Both experimental [5,25] and theoretical [26–28] investigations on nanotwinned metals suggest that twin boundaries beneficially act as barriers to slip (i.e., dislocation motion) but deleteriously act as nucleation sites for partial dislocations. The balance of the effects of slip barriers and dislocation-nucleation sites is material-dependent and ultimately dictates λ_{cr} . Importantly, recognize that this mechanism was developed for metals. Ceramics, on the other hand, have strong chemical bonds that largely counter slip [29]. Regardless, some still argue that nanotwinning benefits ceramics by resisting slip [7,29]. Others argue that nanotwinning beneficially increases quantum confinement of bandgap energy of ceramics [7,30]. Few investigations of nanotwinned ceramics are available, so the correct mechanism may not have been speculated yet.

Determining λ_{cr} for B₆O represents a first step in demystifying the mechanism of nanotwinning in ceramics and in potentially achieving record properties for boron suboxide. To begin, a prior work established a new nomenclature for B₆O [14]. They retained the name of α -B₆O for the non-twinned structure but discarded β -B₆O and nt-B₆O for the nanotwinned structure. Instead, they proposed $i\tau$ -B₆O where i represents the number of layers of icosahedra between twin boundaries. For example, τ -B₆O has twin boundaries separated by a single layer of icosahedra and a λ of approximately $0.44 \,\mathrm{nm}$ [Fig. 1(c)]. Likewise, 2τ -B₆O has twin boundaries separated by two layers of icosahedra and a λ of approximately 0.89 nm [Fig. 1(d)]. That study also found that the DFT ground-state static energies of α -B₆O, τ -B₆O, 2τ -B₆O, 3τ -B₆O, and 4τ -B₆O were essentially equivalent. Therefore, we predict that experimentally varying twin spacing is feasible and that a fabricated sample could contain multiple regions with dissimilar twin spacings.

Apart from nanotwinning at critical spacing, countering solidstate amorphization represents the principal concern for maximizing the mechanical strength of many boron-rich icosahedral solids, including B_6O . In this deleterious mechanism, high pressures induce disordered bands at the nanoscale to concentrate stress and promote microcracking, post-yield softening, and catastrophic failure [17]. Before the present work, only two studies have experimentally observed amorphization of B_6O . They showed that nanoindentation induced amorphous bands with a width of 2–3 nm and a length of 200–300 nm mostly along $\{0\overline{1}11\}$ and $\{\overline{1}012\}$ [15,31]. Although no other experimental works covered the amorphization of B_6O , similarly sized amorphous bands were frequently found in B_4C [17,32–34]. In contrast to amorphization of B_6O , however, the amorphous bands in B_4C lay along numerous planes: $(11\overline{2}3)$ and $(2\overline{1}1\overline{3})$ for ballistic impact [32], $(21\overline{3}5)$ and $(2\overline{2}01)$ for laser shock [35], $(31\overline{4}0)$ for hydrostatic depressurization [36], and many planes for indentation [33,37]. We believe this variety of preferred directions in B_4C is due to its aforementioned polymorphism-driven heterogeneity. Therefore, we expect less variety in the preferred directions for B_6O , which is much more homogeneous crystallographically. Regardless, the origins of amorphization, especially for B_6O , remain unclear.

The objective of this manuscript is to characterize and rationalize the mechanical response of nanotwinned B₆O. We first present the results of pulse-echo ultrasound, quasistatic/dynamic indentation, and quasistatic compression for both hot-pressed (HP) and spark-plasma-sintered (SPS) samples. To our knowledge, this is the first dynamic testing of B₆O. With scanning electron microscopy (SEM) and high-resolution transmission electron microscopy (HR-TEM), we explain the trends in properties through measurements of porosity, grain size, nanotwinning, and amorphization. We demonstrate that the twins and amorphous bands in B₆O heavily prefer certain crystallographic planes. We also employ Raman spectroscopy to investigate the uniqueness of the amorphization of B₆O. With experimental and quantum mechanical x-ray diffraction (XRD), we present a potential tool for quantifying the volume fraction of nanotwinning, which we believe to be beneficial to mechanical response. Finally, we perform biaxial shear simulations to suggest the critical twin spacing specific to B₆O.

2. Experimental

2.1. Materials

This study covers the two most popular high-pressure-high-temperature (HPHT) processing techniques for polycrystalline ceramics: hot pressing (HP) and spark plasma sintering (SPS). While both techniques mechanically apply uniaxial pressure, HP and SPS apply temperature through radiation and conduction, respectively. This difference in heating mechanism makes SPS significantly faster than HP and therefore can produce microstructural differences. The

HP sample was produced with a peak temperature of 1850 °C, peak pressure of 50 MPa, and total time of 2 h. The SPS sample was produced with a peak temperature of 1600 °C, peak pressure of 55 MPa, and total time of 15 min. Starting powder for both samples was obtained from the sole provider: Fraunhofer Institute for Ceramic Technologies and Systems. After processing, both samples were ground and cut into rectangular prisms measuring $3.4 \times 3.4 \times 5.0$ mm. Because processing methods for B₆O are still unrefined, the grinding and cutting revealed severe cracking in both materials. Hence, only a few intact samples were extracted for mechanical testing.

2.2. Indentation, compression, and ultrasound

Both HP and SPS samples were polished to a 1- μ m surface finish with lapping under maximum pressures of 40 N for 50 min. Quasistatic indentation (i.e., $\approx 10^{-3} \ s^{-1}$) was performed with a Wilson Instruments Instron Tukon [®] 2100B hardness tester with a Vickers indenter and loads ranging from 0.98 to 14.7 N. Dynamic indentation (i.e., $\approx 10^{+3} \ s^{-1}$) was performed with a Vickers indenter and a custom dynamic hardness tester that uses a momentum trap to ensure single indentations within a hundred microseconds [38]. For these dynamic tests, load was stochastically varied from 2.40 to 17.3 N. To facilitate direct comparison of the quasistatic and dynamic tests and to standardize measurements across investigations, we computed slope hardness (HV_{GPa}) [18,39], which is given by the slope of Eq. (1). Here, P_N is the indentation load in N, and d_{mm} is the average indentation diagonal in mm.

$$0.0018544 P_N = (HV_{GPa})d_{mm}^2 (1)$$

Limited sample size precluded fracture-toughness testing using Chevron-notch specimens. Instead, we approximated fracture toughness from indentation-induced radial cracks. This technique may suffer error up to 25% [40,41] but provides a common semi-quantative comparison of materials. At low loads, radial cracks were either non-existent or unmeasurable in scanning electron microscopy. At high loads, the diversion of some energy from radial cracking to lateral cracking induced error in the toughness calculation. Hence, the tip-to-tip lengths of the radial cracks (2c) and diagonals (2a) from 9.8-N indents were measured and substituted into Eq. (2), which is one of several empirical estimates of fracture toughness (K_{IC}) [42].

$$K_{IC} = 0.16(c/a)^{-1.5} HVa^{1/2}$$
 (2)

Due to limited number of samples, quasistatic compression was performed on a single sample of HP B_6O with a TestResources Model 314-150 with a 222-kN (50-klbf) load cell. To avoid indentation of the small ceramic sample into the metal platens, tungstencarbide (WC) inserts were placed around the sample in the loading column

The mass densities of the HP and SPS samples were obtained by performing Archimedes' method on several rectangular specimens. We measured elastic moduli through pulse-echo ultrasound with an Olympus 5072PR pulser/receiver, Olympus longitudinal/shear piezoelectric transducers, and an InfiniiVision® MSO-X 2012A Mixed-Signal Oscilloscope.

2.3. Electron microscopy

Microstructural observations of porosity, phase composition, and fracture patterns were made on a FEI Nova NanoSEM 430. Because B_6O is highly resistant to thermal and chemical etching, grain size was approximated from micrographs of fracture surfaces

induced by 300-N indentations. Because observation of nanotwinning, amorphization, and other crystallographic defects required higher magnification, HR-TEM was performed on a JEOL 2010F with a 200-kV accelerating voltage and a Gatan Orius SC200B camera. TEM samples were prepared from both virgin and indented (0.98 N, Vickers) regions on an FEI Helios Nanolab 600 with an Omniprobe Autoprobe 200. Because of the hexagonal crystal structures, $\pm [1120]$ was chosen for the zone axis for TEM imaging.

2.4. Raman spectroscopy

For B₄C, several studies suggested that volume of amorphized material can be correlated to the intensities of the Raman peaks at 1340 (i.e., "D" peak), 1580 (i.e., "G" peak), and 1820 cm⁻¹ [17,32–34]. In particular, tracking the 1340-cm⁻¹ peak produced by a 532-nm laser is popular. Because Raman-active vibrational modes require bonding, considerable debate questions why new Raman peaks (i.e., new bonding characteristics) accompany amorphization (i.e., a loss of bonding). Regardless, to investigate if this quick and non-destructive technique could track amorphization in B₆O as well, Raman spectroscopy was performed on virgin and indented regions of HP and SPS B₆O with a Renishaw InVia® Raman spectrometer. A prior experimental investigation [43] indicated that red and green lasers induce fluorescence in B₆O, so both 325-nm (i.e., ultraviolet) and 532-nm (i.e., green) lasers were used.

2.5. X-ray diffraction

As nanotwinning was previously shown to minimally affect the static energy of B_6O [14], experimental samples likely contain a mixture of $\alpha\text{-}B_6O$ and nt- B_6O . This coexistence of $\alpha\text{-}B_6O$ and nt- B_6O is supported by the HR-TEM images presented in the results section. Therefore, an efficient means of quantifying the volume of nanotwinned material would be useful for processing investigations that seek to optimize nanostructure for mechanical response. HR-TEM can detect nanotwinning when appropriately aligned but is time-consuming and only probes a small volume. Therefore, we performed x-ray diffraction (XRD) on a PANalytical X'Pert $^{3(8)}$ Powder XRD system. This bulk measurement should be able to nondestructively detect and perhaps quantify the twin boundaries in a sample of B_6O .

For comparison to the experimental XRD scans, we also performed quantum mechanical (QM) simulations of α -B₆O, τ -B₆O, and 2τ-B₆O. First, we obtained the relaxed atomic positions and lattice parameters from density functional theory (DFT). For the smaller systems (i.e., α -B₆O and τ -B₆O), we used the ABINIT[®] software [44-46] with plane-wave-basis sets, periodic boundaries, Troullier-Martins norm-conserving pseudopotentials, the Teter-Pade local-density approximation (LDA) of the exchangecorrelation functional [46], and a 1900-eV cutoff energy. We had previously used these parameters to successfully calculate static energies and relative abundances of B₄C polymorphs in HP and SPS samples [21,47]. For the large-atom system (i.e., 2τ - B_6 O), we used the Vienna Ab initio Simulation Package (VASP) [48-51] with plane-wave-basis sets, periodic boundaries, the projectoraugmented-wave (PAW) method, the Perdew-Burke-Ernzerhof (PBE) exchange-correlation functional, and a 600-eV cutoff energy. After computing ground-state configurations (i.e., the relaxed atomic positions and lattice parameters) for all three structures, XRD spectra were simulated with the CrystalDiffract® software.

2.6. Biaxial shear

To help determine the critical twin spacing of B_6O , we simulated biaxial shear deformations parallel to the twin boundary [i.e.,

(001)/<100> in the rhombohedral system] on structures with one [i.e., τ -B₆O, $\lambda \approx 0.44$ nm, Fig. 1(c)], two [i.e., 2τ -B₆O, $\lambda \approx 0.89$ nm, Fig. 1(d)], and four (i.e., 4τ -B₆O, $\lambda \approx 1.75$ nm) layers of icosahedra between twin boundaries. Biaxial shear approximates the complex stress state under indentation experiments [14,52]. To mimic a Vickers indenter, we set $_{ZZ} =_{ZX} \tan(68^\circ)$ and relaxed strains in the other directions [14,52]. For this biaxial shear, we used the Vienna Ab initio Simulation Package (VASP) [48–51] with the aforementioned computational parameters.

3. Results

Table 1 compares the results of the indentation, compression, and ultrasonic testing of HP B₆O and SPS B₆O to those from a prior study on SPS B₄C [18]. First, see that all three materials exhibited strain-rate hardening (i.e., the dynamic properties superseded the quasistatic ones for a given material). Most importantly, see that for most mechanical properties, SPS B₆O outperformed the other two materials. At both quasistatic and dynamic strain rates, the hardness of SPS B₆O superseded those of SPS B₄C and HP B₆O by significant margins. For approximate fracture toughness, which may have large uncertainty outside the standard error reported in Table 1 (e.g., from differences in measurement method), SPS B₆O surpassed its hot-pressed variant by 10% but lost to B₄C by 8%. For quasistatic strength, HP B₆O dominated SPS B₄C by almost 40%. This extraordinary 5-GPa strength is the highest ever reported for B₆O. Limitation of number of SPS-B₆O specimens precluded measurement of the quasistatic strength of SPS B₆O, but its superior hardness and fracture toughness suggest a strength even higher than that of HP B₆O. Finally, all elastic moduli were significantly higher for SPS B₆O than the other two materials. Hence, our mechanical testing demonstrated not only the promise of B₆O but also the advantage of SPS.

The SEM micrographs of the fracture surfaces (Fig. 2) show that both samples benefited from phase uniformity (i.e., no major secondary phases) but that HP produced more porosity than SPS. This finding is consistent with the relative densities of the HP and SPS samples in Table 1. Assuming a theoretical density of 2.68 g/cm³ (i.e., the value from our ground-state DFT simulations), HP and SPS B₆O achieved 96% and 99% mass density, respectively. This porosity disparity could contribute to the differences in elastic moduli, yield strength, hardness, and fracture toughness. For example, see that a 3% difference in porosity (i.e., 96% vs. 99% mass density) correlated with a 13% drop in Young's modulus (i.e., 484 vs. 427 GPa). This observation is consistent with a prior study that revealed a 5% drop in Young's modulus for approximately each percent of porosity in zirconia, another hard ceramic [53]. Finally, the SEM images reveal that the two B₆O samples had the same grain size as the previously studied SPS B₄C (i.e., 300 nm) [18]. Hence, differences in Table 1 cannot be attributed to grain size.

Fig. 3 presents representative HR-TEM images of virgin B₆O.

Table 1 Experimental properties show the superiority of SPS B_6O over HP B_6O and SPS B_6C . Reported hardness values are independent from the indentation load through the slope-hardness calculation.

Experimental Property	HP B ₆ O	SPS B ₆ O	SPS B ₄ C [16]
Quasistatic Hardness (HV _{OS} GPa)	27.0 ± 0.3	29.9 ± 0.4	29.3 ± 0.3
Dynamic Hardness (HV _D , GPa)	29.5 ± 0.5	31.8 ± 0.5	29.9 ± 0.7
Quasistatic Toughness (K _{IC} , MPa·m ^{1/2})	2.77 ± 0.04	3.15 ± 0.05	3.4 ± 0.1
Quasistatic Strength (σ_{QS} , GPa)	5.0	N/A	3.6 ± 0.2
Bulk Modulus (K, GPa)	203	243	229
Shear Modulus (G, GPa)	186	207	186
Elastic Modulus (E, GPa)	427	484	460
Mass Density (, g/cm ³)	2.57	2.64	2.50

Consistent with the SEM images, Fig. 3(a) indicates a grain size of approximately 300 nm. As shown by Fig. 3(b) and (c), both samples exhibited heterogeneous nanotwinning. For regions with the densest twinning (see figure inserts), HP B₆O had double the twin spacing of SPS B₆O (i.e., 2 vs. 1 nm). As proposed in the Discussion section, nanotwin spacing could affect hardness, toughness, and strength (see Table 1). However, nanotwinning generally does not affect elasticity (see Introduction) so cannot account for the differences in moduli. Regardless of processing method, twins and faults were found along (0111) as in previous studies [15,31] and in contrast to B₄C, which had many more preferred directions (see Introduction).

Fig. 4(a) shows that indentation induced amorphous bands within a depth of two microns from the indented surface. These bands were only a few nanometers in width but extended over several hundred nanometers in length. At this low magnification, the growth of these bands seems randomly oriented as in B_4C . However, higher magnification shows that the nucleation of these bands was preferentially along $(01\overline{12})$. Fig. 4(b) and (c) show that these amorphous bands can shear apart twins along $[0\overline{1}11]$ by up to a few nanometers (see dotted lines). This deformation highlights the shear-driven nature of amorphization.

Although the HR-TEM clearly indicated the presence and distribution of amorphous bands, tremendous effort is required to sample a large region. To evaluate if Raman spectroscopy can track amorphization, Fig. 5 presents the Raman spectra of virgin and indented samples of B_6O probed by a 325-nm laser (note: the 532-nm Raman scans had similar features but excessive fluorescence). The scans of the virgin HP and SPS B_6O differ mostly by intensities at 330, 790 and $1290\,\mathrm{cm}^{-1}$ [see Fig. 5(a)]. This observation parallels the fact that HP and SPS B_4C differ by the Raman intensities around 265, 320, 480, 533, and $825\,\mathrm{cm}^{-1}$ [21]. However, this similarity of the trends in Raman spectra of B_4C and B_6O did not extend to amorphization. While three new Raman peaks appear in amorphized B_4C [17], the Raman spectra of virgin and indented B_6O are nearly identical [see Fig. 5(b) and (c)]. Hence, Raman spectroscopy can efficiently track amorphization in B_4C but not in B_6O .

Unlike Raman spectroscopy, XRD cannot easily differentiate HP and SPS B₆O [see Fig. 6(a)]. To assess if XRD can quantify volume of nanotwinned material, Fig. 6(b) - (d) present the simulated x-ray diffractions of α -B₆O, τ -B₆O, and 2τ -B₆O. See that the simulated XRD pattern of α -B₆O [Fig. 6(b)] captures all of the features of the experimental scan [Fig. 6(a)]. This similarity suggests that the heterogeneous nanotwinning revealed by the HR-TEM [see Fig. 3(b) and (c)] occupies a negligible volume fraction of the fabricated samples. This finding is consistent with the fact that the experimental hardness values of B₆O were not excessively larger than those of B₄C [see Table 1]. Interestingly, see that the simulated XRD spectra of τ -B₆O and 2τ -B₆O have only minor differences, which may be due to differences in software (i.e., ABINIT vs. VASP) and parameters (e.g., exchange-correlation functional). Most importantly, a strong peak at 2 ≈ 37 exists for both nanotwinned structures but not for α -B₆O. Hence, we propose that this peak could be used to track the volume fraction of nanotwinning in fabricated B₆O.

From the stress-strain curves for the biaxial shear [Fig. 7(a)], the critical (i.e., maximum) stress of 2τ -B₆O (i.e., 37.8 GPa) exceeded than that of τ -B₆O (i.e., 36.2 GPa) and 4τ -B₆O (i.e., 36.3 GPa). Likewise, the energy (i.e., area under the stress-strain curve up to critical stress) is highest for 2τ -B₆O by over 15%. Hence, the deformation of 2τ -B₆O is most difficult, and the ideal twin spacing (λ_{cr}) for B₆O is likely around 0.89 nm. We note that this ideal twin spacing was achieved in the heavily nanotwinned regions of the fabricated SPS B₆O [see Fig. 1(c)]. Although other factors may be at play, especially heterogeneous nanotwinning and porosity, note

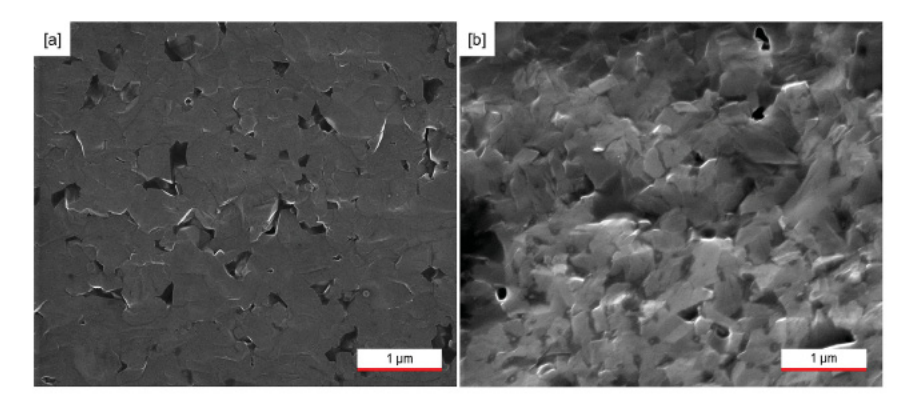


Fig. 2. Fracture surfaces of (a) HP B₆O and (b) SPS B₆O reveal porosity and a 300-nm grain size.

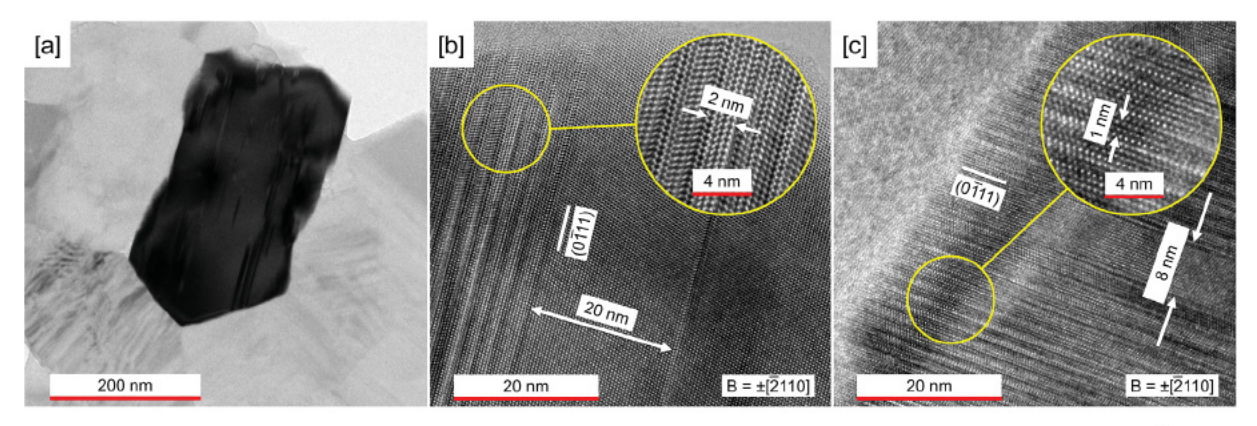


Fig. 3. Representative HR-TEM of virgin B_6O shows (a) 300-nm grain size, (b-c) heterogeneous nanotwin spacing, and (b-c) a preferred twinning plane of $(0\overline{1}11)$. Minimum twin spacing is larger in (b) HP B_6O than in (c) SPS B_6O .

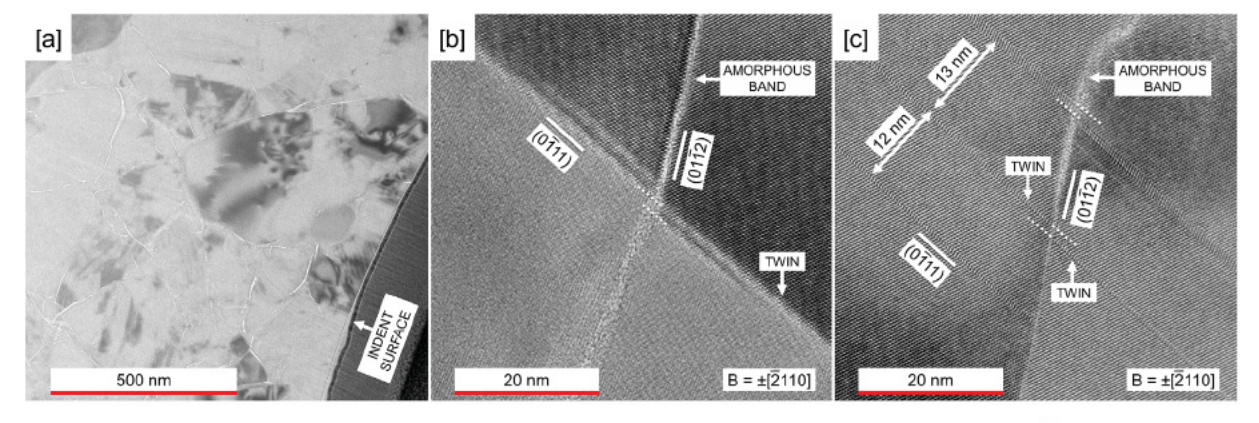


Fig. 4. Representative HR-TEM of indented B_6O shows (a) an indentation profile with cracking and (b-c) amorphous bands primarily along (01 $\overline{12}$). These bands can shear apart the twins (see dotted lines) and were only found in regions with large twin spacing.

that the ideal twin spacing coincides with the superior properties in Table 1. Understanding why this nanotwin spacing may be ideal is complicated by the absence of a consensus on the mechanisms by which nanotwinning affects ceramics and by potential limitations of the computational modeling. Hence, we provide new arguments for this strengthening mechanism in the Discussion section.

4. Discussion

Recall from the Introduction that for metals, nanotwins are thought to beneficially resist slip but deleteriously promote formation of partial dislocations. Although slip is typically far more difficult in ceramics than in metals, some still argue that these materials may share the same mechanisms. For example, see that the twin boundaries (i.e., sites susceptible to partial dislocations) are most numerous in τ -B₆O and are close together at critical stress [see Fig. 7(b)]. Perhaps proximity of these dislocation-nucleation sites promotes the formation of enough dislocations to counter the benefits of the increased number of barriers to slip. Alternatively, 2τ -B₆O has an entire layer of icosahedra between the twin boundaries to avoid interaction of the partial-dislocation sites but still benefits from barriers to slip [see Fig. 7(c)]. Adding another two layers of

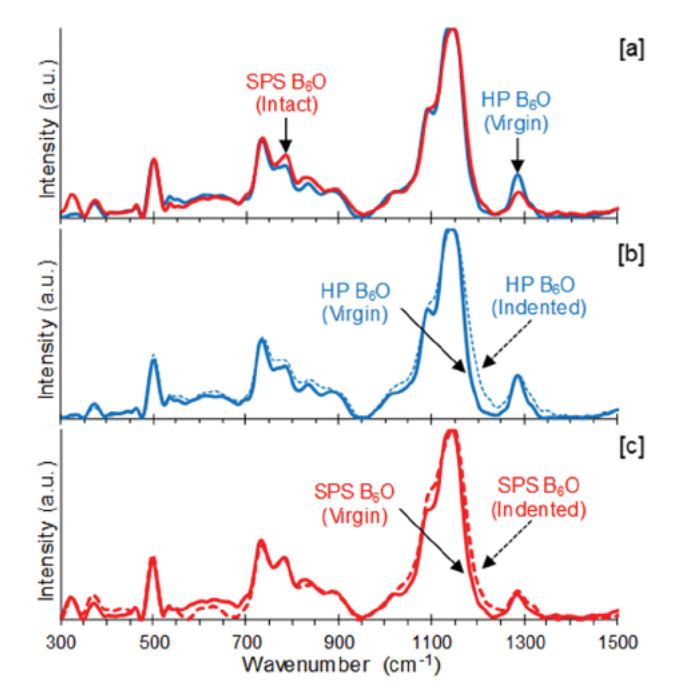


Fig. 5. (a) Raman spectra (325-nm laser) of virgin HP and SPS differ mostly by intensities of the peaks at 330, 790, and $1290\,\mathrm{cm^{-1}}$. Indentation has little effect on Raman spectrum for both (b) HP B_6O and (c) SPS B_6O .

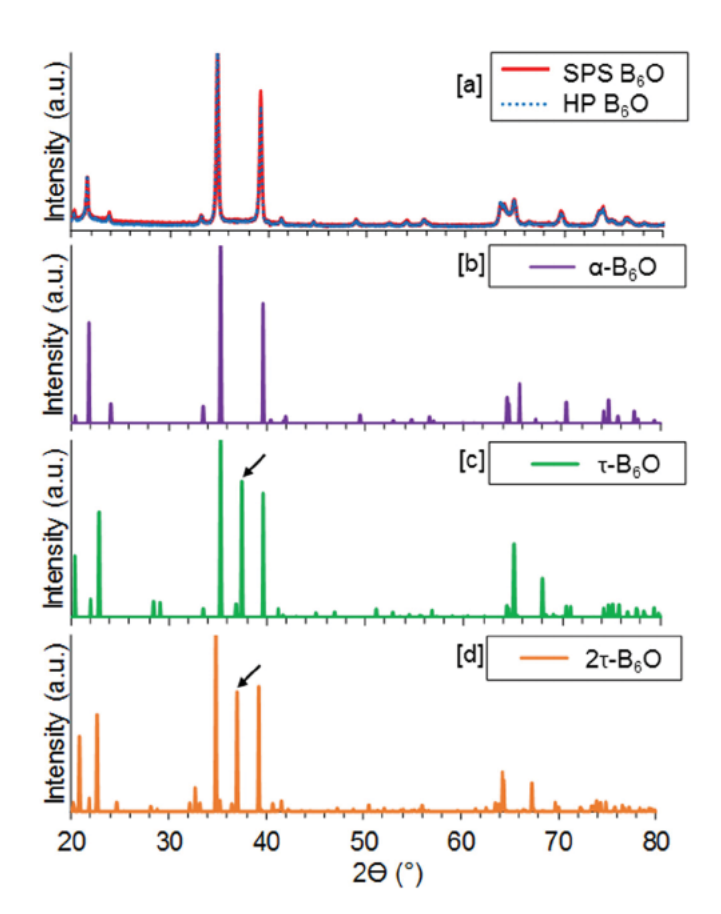


Fig. 6. X-ray diffraction (XRD) of (a) experimental B_6O , (b) simulated α - B_6O , (c) simulated τ - B_6O (i.e., β - B_6O), and (c) simulated 2τ - B_6O suggest limited nanotwinning in experimental samples. The unique peak at 2 $=37^\circ$ in τ - B_6O and 2τ - B_6O correlates with nanotwinning regardless of twin spacing.

icosahedra between twin boundaries in 4τ -B₆O may merely reduce the number of barriers to slip without significantly further reducing the interaction of partial-dislocation sites [see Fig. 7(d)].

In light of the fact that dislocations typically initiate cracks rather than slip in ceramics, perhaps the twin boundaries beneficially resist the growth of cracks and/or amorphous bands instead of slip. After all, nanotwinning and nanograining share characteristics, such as a lack of influence on elastic properties. For nanograining, the variation of fracture toughness with grain size is often explained with crack deflection. Maybe nanotwins work in a similar way to arrest/divert growth of cracks or even the amorphous bands that are thought to initiate cracks. The fact that amorphous bands were exclusively found in non-twinned or lightly twinned regions in the HR-TEM [e.g., Fig. 4] supports this idea.

Testing this theory that twin boundaries resist the growth of cracks and/or amorphous bands, however, requires expensive computational modeling different from the high-periodicity models of the current investigation. Cracks and amorphous bands relieve stress locally so would likely be spread out. Hence, development of molecular-dynamics potentials to enable simulation of larger cells may prove useful. Also, a fundamental model for the amorphization of B₆O would be needed to properly simulate the effect of twin boundaries on the growth of amorphous bands. Most predict that amorphization is the dominant failure mechanism for many icosahedral solids [31e33], [54], but the specifics of the mechanism are frequently debated. The amorphization of B4C is most studied [33], but the results of the current investigation seem to suggest that the amorphization of B₆O is unique. The HR-TEM revealed that the amorphous bands formed along much fewer number of directions in B₆O than in B₄C. This finding suggests that the deformation of B₆O is much more ordered than that of B₄C. Also, amorphization altered the Raman spectrum of B₄C [17] but not of B_6O (see Fig. 5). This finding suggests that the bonding in B_6O changes differently than in B₄C when deformed.

We attribute these amorphization differences between B_4C and B_6O to crystal structure. In the most abundant polymorph of B_4C , the serially bonded, C-B-C chain [see Fig. 1(a)] is susceptible to bending that has been theorized to initiate amorphization [55,56]. On the contrary, the two oxygen atoms that bond icosahedra in B_6O are not bonded serially, and there is no easily displaceable central chain atom [Fig. 1(b)]. Further, B_4C suffers from structural heterogeneity due to polymorphism [21] while B_6O does not. Polymorphism-induced differences in adjacent cell volumes have been theorized to affect stability [57]. Overall, we believe these structural differences allow the amorphization in B_6O to be different from that of B_4C . Therefore, we recommend future studies on experimentally tracking and theoretically modeling the unique amorphization of B_6O .

Regardless of modeling difficulty, we assert that B₆O is highly susceptible to nanotwinning. The highly ordered nature of nanotwinning likely requires a crystal structure with little crystallographic variability. B6O is largely immune to polymorphism and substitutional disorder, and the current HR-TEM showed twins and amorphous bands along few directions. Consistent with prior modeling of the static energies of α -B₆O and nt-B₆O [11,13,14], the current HR-TEM also experimentally showed nanotwinning in B₆O. Unfortunately, the properties of our experimental samples (see Table 1) were likely limited by porosity (see Fig. 2) and non-critical twin spacing (see Fig. 3). Therefore, we suggest future work focused on the careful control of processing kinetics (e.g., selection of starting powder and processing parameters) After all, nt-c-BN [7] and nt-D [9] were only fabricated after starting from onion-like nanoparticles. To guide processing of nt-B₆O, we recommend tracking the XRD peak at 37°, which likely indicates the abundance of nanotwinning (see Fig. 6).

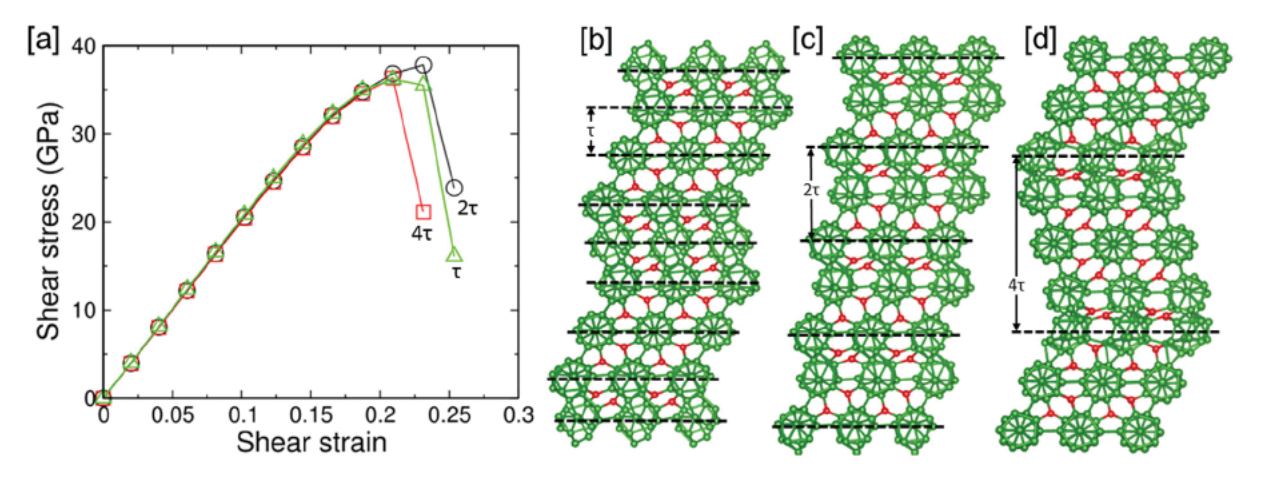


Fig. 7. (a) Stress-strain curves for biaxial shear deformation of τ -B₆O (σ_{cr} = 36.2 GPa), 2τ -B₆O (σ_{cr} = 37.8 GPa), and 4τ -B₆O (σ_{cr} = 36.3 GPa) suggest 2τ -B₆O has λ_c . Structures at critical stress are shown for (b) τ -B₆O, (c) 2τ -B₆O, and (d) 4τ -B₆O. Dotted lines indicate twin planes.

5. Conclusions

Through mechanical, structural, and spectral characterizations, we demonstrated the promise and uniqueness of B₆O, especially with respect to B₄C. For example, quasistatic compression revealed a strength of over 5 GPa, which is both a record for B₆O and superior to that of B₄C. The HR-TEM demonstrated heterogeneous nanotwinning at non-ideal twin spacing and amorphous bands along few directions. Because nanotwinning has set mechanical records for other ceramics, the TEM suggests high potential of B₆O as a structural ceramic. Raman spectroscopy was also performed to demonstrate the uniqueness of B₆O's amorphization as opposed to that of B₄C. To guide future investigations in exploiting nanotwinning in B₆O, quantum mechanical simulations were performed to predict the critical twin spacing (i.e., $\lambda_c = 0.89$ nm) and develop a tool for tracking volume fraction of twinning (i.e., x-ray diffraction \approx 37°). Overall, these findings support the uniqueness and promise of boron suboxide as a superhard superhard material. They also significantly advance the field toward the ultimate goal of determining the exact mechanism by which nanotwinning influences structural ceramics.

Acknowledgements

This work is supported by the Department of the Army [W91CRB-16-C-0035], the Army Research Office [ARO-W911NF-14-1-0230 and W911NF-18-1-0040], National Science Foundation [DGE-1315138 (GRFP: Graduate Research Fellowship Program), ACI-1053575 TG-MSS15006 (XSEDE: Extreme Science and Engineering Discovery Environment), CMMI-1727428], and the US Nuclear Regulatory Commission [NRC-HQ-84-15-G-0028]. We recognize the experimental work of Matthew DeVries (SEM, dynamic indentation), Alison Trachet (XRD), and Andres Trucco (SEM). We acknowledge the Herbert Wertheim College of Engineering Research Service Centers for use of transmission electron microscope, scanning electron microscope, and focused ion beam.

References

- [1] J. Christian, S. Mahajan, Deformation twinning, Prog. Mater. Sci. 39 (1995) 1–157.
- [2] Z. Zhao, B. Xu, Y. Tian, Recent advances in superhard materials, Annu. Rev. Mater. Res. 46 (2016) 383–406.
- [3] T. Zhu, J. Li, Ultra-strength materials, Prog. Mater. Sci. 55 (2010) 710-757.
- [4] L. Lu, Y. Shen, X. Chen, L. Qian, K. Lu, Ultrahigh strength and high electrical conductivity in copper, Science 304 (2004) 422–426.

- [5] L. Lu, X. Chen, X. Huang, K. Lu, Revealing the maximum strength in nanotwinned copper, Science 323 (2009) 607–610.
- [6] N.M. Heckman, M.F. Berwind, C. Eberl, A.M. Hodge, Microstructural deformation in fatigued nanotwinned copper alloys, Acta Mater. 144 (2018) 138–144
- [7] Y. Tian, B. Xu, D. Yu, Y. Ma, Y. Wang, Y. Jiang, et al., Ultrahard nanotwinned cubic boron nitride, Nature 493 (2013) 385—388.
- [8] N. Dubrovinskaia, L. Dubrovinsky, Controversy about ultrahard nanotwinned cBN, Nature 502 (2013) E1–E2.
- [9] Q. Huang, D. Yu, B. Xu, W. Hu, Y. Ma, Y. Wang, et al., Nanotwinned diamond with unprecedented hardness and stability, Nature 510 (2014) 250–253.
- [10] Q. An, Prediction of superstrong 7-boron carbide phase from quantum mechanics, Phys. Rev. B. 95 (2017) 100101.
- [11] Q. An, W.A. Goddard, K.Y. Xie, G. Sim, K.J. Hemker, T. Munhollon, et al., Su-perstrength through nanotwinning, Nano Lett. 16 (2016) 7573–7579.
- [12] K.Y. Xie, Q. An, M.F. Toksoy, J.W. McCauley, R.A. Haber, W.A. Goddard III, et al., Atomic-level understanding of "asymmetric twins" in boron carbide, Phys. Rev. Lett. 115 (2015) 175501.
- [13] H. Dong, A.R. Oganov, Q. Wang, S.N. Wang, Z. Wang, J. Zhang, et al., Prediction of a new ground state of superhard compound B6O at ambient conditions, Sci. Rep. 6 (2016) 31288.
- [14] Q. An, K.M. Reddy, H. Dong, M. Chen, A.R. Oganov, W.A. Goddard, Nanotwinned boron suboxide (B6O): new ground state of B6O, Nano Lett. 16 (2016) 4236–4242
- [15] Q. An, K.M. Reddy, J. Qian, K.J. Hemker, M. Chen, W.A. Goddard III, Nucleation of amorphous shear bands at nanotwins in boron suboxide, Nat. Commun. 7
- [16] M. Herrmann, I. Sigalas, M. Thiele, M.M. Muller, H.J. Kleebe, A. Michaelis, Boron suboxide ultrahard materials, Int. J. Refract. Met. H. 39 (2013) 53–60.
- [17] V. Domnich, S. Reynaud, R. Haber, M. Chhowalla, Boron carbide: structure, properties, and stability under stress, J. Am. Ceram. Soc. 94 (2011) 3605—3628
- [18] M. DeVries, J. Pittari, G. Subhash, K. Mills, C. Haines, J.Q. Zheng, Rate-dependent mechanical behavior and amorphization of ultrafine-grained boron carbide, J. Am. Ceram. Soc. 99 (2016) 3398–3405.
 [19] I. Solodkyi, D. Demirskyi, Y. Sakka, O. Vasylkiv, Hardness and toughness
- [19] I. Solodkyi, D. Demirskyi, Y. Sakka, O. Vasylkiv, Hardness and toughness control of brittle boron suboxide ceramics by consolidation of star-shaped particles by spark plasma sintering, Ceram, Bar Int. (2016).
- [20] D. Demirskyi, I. Solodkyi, Y. Sakka, O. Vasylkiv, H. Kleebe, High-temperature strength of boron suboxide ceramic consolidated by spark plasma sintering, I. Am. Ceram. Soc. 99 (2016) 2769–2777.
- [21] C. Kunka, A. Awasthi, G. Subhash, Evaluating boron-carbide constituents with simulated Raman spectra, Scr. Mater. 138 (2017) 32–34.
- [22] H. Hubert, B. Devouard, L.A. Garvie, M. O'Keeffe, P.R. Buseck, W.T. Petuskey, et al., Icosahedral packing of B12 icosahedra in boron suboxide (B6O), Nature 391 (1998) 376–378.
- [23] T. Fujita, P. Guan, K. Madhav Reddy, A. Hirata, J. Guo, M. Chen, Asymmetric twins in rhombohedral boron carbide, Appl. Phys. Lett. 104 (2014) 021907.
- [24] C. Cheng, K.M. Reddy, A. Hirata, T. Fujita, M. Chen, Structure and mechanical properties of boron-rich boron carbides, J. Eur. Ceram. Soc. 37 (2017) 4514–4523.
- [25] D. Jang, X. Li, H. Gao, J.R. Greer, Deformation mechanisms in nanotwinned metal nanopillars, Nat. Nanotech 7 (2012) 594–601.
- [26] X. Li, Y. Wei, L. Lu, K. Lu, H. Gao, Dislocation nucleation governed softening and maximum strength in nano-twinned metals, Nature 464 (2010) 877–880.
- [27] K. Lu, L. Lu, S. Suresh, Strengthening materials by engineering coherent internal boundaries at the nanoscale, Science 324 (2009) 349–352.
- [28] A. Stukowski, K. Albe, D. Farkas, Nanotwinned fcc metals: strengthening

- versus softening mechanisms, Phys. Rev. B. 82 (2010) 224103.
- [29] X. Li, S. Yin, S.H. Oh, H. Gao, Hardening and toughening mechanisms in nanotwinned ceramics, Scr.Mater 133 (2017) 105–112.
- [30] S.T. John, D.D. Klug, F. Gao, Hardness of nanocrystalline diamonds, Phys. Rev. B. 73 (2006) 140102.
- [31] K. Reddy, A. Hirata, P. Liu, T. Fujita, T. Goto, M. Chen, Shear amorphization of boron suboxide, Scr. Mater. 76 (2014) 9-12.
- [32] M. Chen, J. McCauley, K. Hemker, Shock-induced localized amorphization in boron carbide, Science 299 (2003) 1563–1566.
- [33] G. Subhash, A. Awasthi, C. Kunka, P. Jannotti, M. DeVries, In search of amorphization-resistant boron carbide, Scr. Mater. 123 (2016) 158-162.
- [34] G. Parsard, G. Subhash, Raman spectroscopy mapping of amorphized zones beneath static and dynamic Vickers indentations on boron carbide, J. Eur. Ceram. Soc. 37 (2017) 1945-1953.
- [35] S. Zhao, B. Kad, B.A. Remington, J.C. LaSalvia, C.E. Wehrenberg, K.D. Behler, et al., Directional amorphization of boron carbide subjected to laser shock compression, Proc. Natl. Acad. Sci. U. S. A. (2016).
- [36] X. Yan, Z. Tang, L. Zhang, J. Guo, C. Jin, Y. Zhang, et al., Depressurization amorphization of single-crystal boron carbide, Phys. Rev. Lett. 102 (2009) 075505
- [37] K.M. Reddy, P. Liu, A. Hirata, T. Fujita, M. Chen, Atomic structure of amorphous shear bands in boron carbide, Nat. Commun. 4 (2013) 2483.
- [38] G. Subhash, Dynamic indentation testing, in: ASM Handbook Volume 8, Mechanical Testing and Evaluation, ASM International, 2000, p. 519.
- [39] J. Pittari, G. Subhash, A. Trachet, J. Zheng, V. Halls, P. Karandikar, The ratedependent response of pressureless-sintered and reaction-bonded silicon carbide-based ceramics, Int. J. Appl. Ceram. Tec. 12 (2015) E207—E216. [40] G.D. Quinn, R.C. Bradt, On the Vickers indentation fracture toughness test,
- Am. Ceram. Soc. 90 (2007) 673-680.
- [41] J.J. Kruzic, R.O. Ritchie, Determining the toughness of ceramics from Vickers indentations using the crack-opening displacements: an experimental study, Am. Ceram. Soc. 86 (2003) 1433-1436.
- [42] E. Rocha-Rangel, Fracture toughness determinations by means of indentation fracture, in: J. Cuppoletti (Ed.), Nanocomposites with Unique Properties and Applications in Medicine and Industry, InTech, 2011, p. 21.

- [43] O.O. Kurakevych, V.L. Solozhenko, Experimental study and critical review of structural, thermodynamic and mechanical properties of superhard refractory boron suboxide B6O, I. Superhard Mater. 33 (2011) 421-428.
- [44] X. Gonze, B. Amadon, P. Anglade, J. Beuken, F. Bottin, P. Boulanger, et al., ABINIT: first-principles approach to material and nanosystem properties, Comput. Phys. Commun. 180 (2009) 2582-2615.
- [45] X. Gonze, A brief introduction to the ABINIT software package, Z. für Kristallogr. - Cryst. Mater. 220 (2005) 558–562.
- S. Goedecker, M. Teter, J. Hutter, Separable dual-space Gaussian pseudopotentials, Phys. Rev. B. 54 (1996) 1703-1710.
- [47] C. Kunka, A. Awasthi, G. Subhash, Crystallographic and spectral equivalence of boron-carbide polymorphs, Scr. Mater. 122 (2016) 82-85.
- [48] G. Kresse, J. Hafner, Ab initio molecular dynamics for liquid metals, Phys. Rev. B. 47 (1993) 558.
- [49] G. Kresse, J. Furthmüller, Efficiency of ab-initio total energy calculations for metals and semiconductors using a plane-wave basis set, Comput. Mater. Sci. 6 (1996) 15-50.
- [50] G. Kresse, J. Furthmüller, Efficient iterative schemes for ab initio total-energy calculations using a plane-wave basis set, Phys. Rev. B. 54 (1996) 11169.
- [51] G. Kresse, D. Joubert, From ultrasoft pseudopotentials to the projector augmented-wave method, Phys. Rev. B. 59 (1999) 1758.
- [52] B. Li, H. Sun, C. Chen, Large indentation strain-stiffening in nanotwinned cubic boron nitride, Nat. Commun. 5 (2014) 4965.
- [53] G. Subhash, S. Nemat-Nasser, Dynamic stress-induced transformation and texture formation in uniaxial compression of zirconia ceramics, J. Am. Ceram. Soc. 76 (1993) 153-165.
- A. Awasthi, G. Subhash, Deformation behavior and amorphization in icosahedral boron-rich ceramics, Prog. Mater. Sci. (2017) (accepted).
- [55] Q. An, W. Goddard, T. Cheng, Atomistic explanation of shear-induced amorphous band formation in boron carbide, Phys. Rev. Lett. 113 (2014).
- [56] Q. An, W. Goddard, Atomistic origin of brittle failure of boron carbide from large-scale reactive dynamics simulations: suggestions toward improved ductility, Phys. Rev. Lett. 115 (2015) 105501.
- [57] E. Betranhandy, N. Vast, J. Sjakste, Ab initio study of defective chains in icosahedral boron carbide B 4 C, Solid State Sci. 14 (2012) 1683-1687.